IOP Publishing Bioinspir. Biomim. 19 (2024) 046011 https://doi.org/10.1088/1748-3190/ad493c

Bioinspiration & Biomimetics

CrossMark

RECEIVED
23 February 2024

REVISED
16 April 2024

ACCEPTED FOR PUBLICATION
9 May 2024

PUBLISHED
24 May 2024

PAPER

Gradients of properties increase the morphing and stiffening performance of bioinspired synthetic fin rays

Saurabh Das[1], **Prashant Kunjam**[1], **Jona Faye Ebeling**[1,2] **and Francois Barthelat**[1,*]

[1] Department of Mechanical Engineering, University of Colorado, 427 UCB, 1111 Engineering Dr, Boulder, CO 80309, United States of America

[2] Department of Nature and Engineering, City University of Applied Sciences Bremen, Hermann-Köhl-Straße 1, 28199 Bremen, Germany

[*] Author to whom any correspondence should be addressed.

E-mail: francois.barthelat@colorado.edu

Keywords: Fish fins, morphing materials, bioinspiration, robotic materials, shape morphing

Abstract

State-of-the-art morphing materials are either very compliant to achieve large shape changes (flexible metamaterials, compliant mechanisms, hydrogels), or very stiff but with infinitesimal changes in shape that require large actuation forces (metallic or composite panels with piezoelectric actuation). Morphing efficiency and structural stiffness are therefore mutually exclusive properties in current engineering morphing materials, which limits the range of their applicability. Interestingly, natural fish fins do not contain muscles, yet they can morph to large amplitudes with minimal muscular actuation forces from the base while producing large hydrodynamic forces without collapsing. This sophisticated mechanical response has already inspired several synthetic fin rays with various applications. However, most 'synthetic' fin rays have only considered uniform properties and structures along the rays while in natural fin rays, gradients of properties are prominent. In this study, we designed, modeled, fabricated and tested synthetic fin rays with bioinspired gradients of properties. The rays were composed of two hemitrichs made of a stiff polymer, joined by a much softer core region made of elastomeric ligaments. Using combinations of experiments and nonlinear mechanical models, we found that gradients in both the core region and hemitrichs can increase the morphing and stiffening response of individual rays. Introducing a positive gradient of ligament density in the core region (the density of ligament increases towards the tip of the ray) decreased the actuation force required for morphing and increased overall flexural stiffness. Introducing a gradient of property in the hemitrichs, by tapering them, produced morphing deformations that were distributed over long distances along the length of the ray. These new insights on the interplay between material architecture and properties in nonlinear regimes of deformation can improve the designs of morphing structures that combine high morphing efficiency and high stiffness from external forces, with potential applications in aerospace or robotics.

1. Introduction

Engineering morphing materials can undergo radical shape change without complex mechanisms, offering attractive properties and functionalities for application in soft robotics [1], medical devices [2], automotive [3], aerospace [4], tissue engineering [5], and food manufacturing processes [6]. Examples of morphing materials include hydrogels [7], shape memory polymers/alloys [8], kirigami [9], hygromorphs [10], liquid crystal elastomers [11], smart piezoelectric composites [4], and mechanical metamaterials [12]. Despite rapid advances in the development of these materials, they still suffer from trade-offs between morphing compliance and structural stiffness: morphing materials based on hydrogels or elastomers undergo large shape change with low actuation force, but they cannot carry large

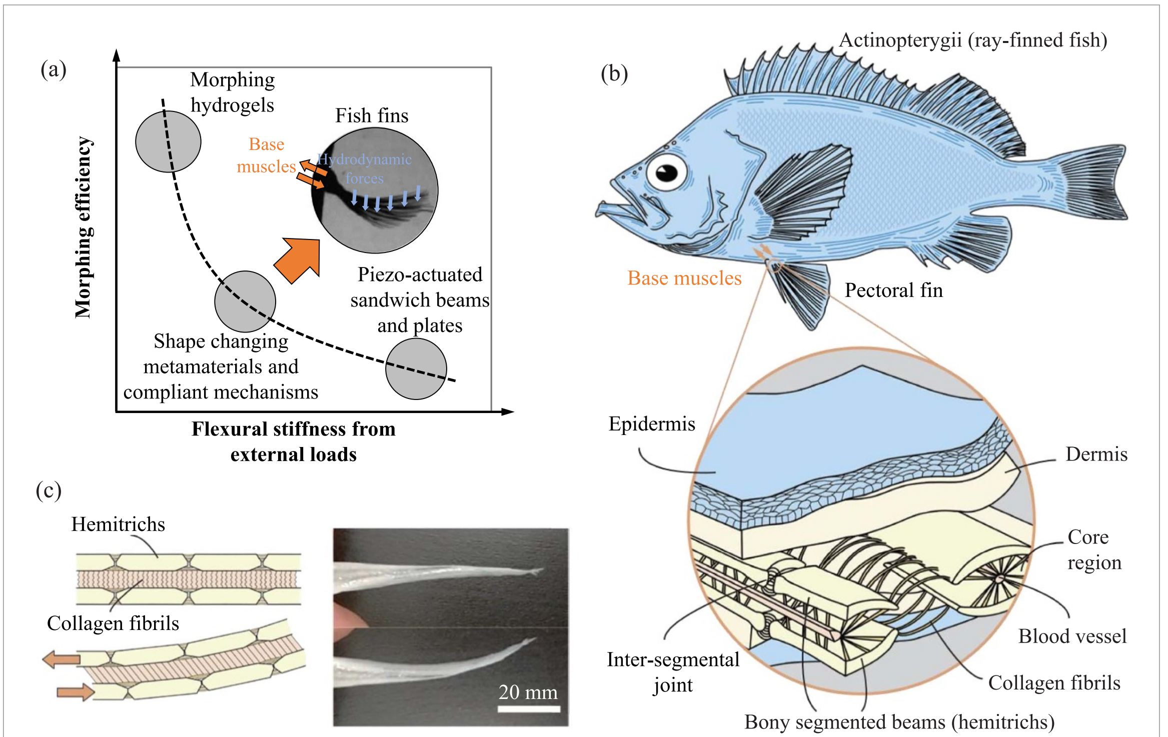

Figure 1. Key features in individual fin rays: (a) fish fins combine high morphing efficiency and high stiffness from external loads, two properties that are mutually exclusive in engineering morphing materials. (b) Typical fins in ray-finned fish and internal structure of the fins; (c) fish can change the shape of their fins from actuation by base muscles. The set of pictures shows an individual ray from a fish fin harvested from Atlantic salmon (*Salmo salar*) that is 'morphed' by applying push/pull forces manually.

external forces [5, 13]. On the other hand, morphing materials based on metals or carbon fiber-reinforced composites are much stiffer, but they require larger actuation forces for relatively small morphing amplitudes [14, 15] (figure 1(a)). The ideal morphing material should simultaneously offer morphing compliance and structural stiffness. Nature abounds in examples of morphing materials, which can serve as inspiration for new designs and morphing strategies that potentially overcome this trade-off [16–19]. Fish fins are notable natural 'stiff' morphing materials. Fish fins are semi-flexible membranes which contain no muscles, and as a result they are often thought of as passive swimming surfaces which are simply 'flapped' for propulsion (caudal fin) or passive stabilization (dorsal fins, pectoral fins). Fish fins are in fact much more sophisticated systems: they display large morphing amplitudes, combined with high stiffness from external loads (hydrodynamic forces), fast response times and actuation from the base only to finely tune hydrodynamic interactions and to generate powerful forces in three dimensions [20]. Fish fins 'probably represents the most elaborate and refined adaptation to efficient interaction with water that has ever evolved' [21] and as such, they can serve as models for the design of new morphing materials. Individual fish fins are composed of a collagenous membrane stiffened by 10–30 beam-like structures called rays. Each ray has a diameter in the order of $\sim$100 μm with a tapered profile and aspect ratio $>$100 (figure 1(b)). The rays are composed of two bony layers called hemitrichs composed of $\sim$300 μm long bony segments. In each ray, the two hemitrichs are connected by a 'core' region composed of collagen fibrils embedded in a ground gel-like substance. A remarkable feature of fish fins is that their curvature can be radically changed solely by muscular actuation from the base of the rays (figure 1(c)). Push/pull actuation induces shear deformations in the core region, while rotations at the base are prevented by the configuration of the tendons and by a cartilaginous pad at the base of the fin. The shear deformation imposed at the base induces competition between the flexural deformation of the hemitrichs and the shear deformation of the core, generating flexural deformations over a long distance over the length of the ray [20, 22–24]. There is a fine balance between the flexural stiffness of the hemitrichs and the shear stiffness of the core, so that the morphing of individual rays involves flexural deformation distributed over the entire length of the ray. Our recent study on individual rays from Rainbow Trout (*Oncorhynchus mykiss*) has shown that the hemitrichs are 3–4 orders of magnitude stiffer than the core region, and that nonlinear mechanical models are required to capture the large deformations and large rotations of individual rays [25].

Fish fins have inspired numerous synthetic materials and structures, for example, 3D printed resin based segmented composite beams [26], propulsion systems for autonomous underwater vehicles (AUVs) [27–30], and soft robotic grippers [31–34]. In addition, fish-like robotic systems based on different types of fish [35–38] and aquatic-aerial vehicles [39–41] have been developed. We have recently designed, fabricated and tested fin ray-like morphing beams with polymethyl methacrylate (PMMA) hemitrichs connected with elastomeric ligaments [42] which duplicated the morphing and stiffening mechanisms of natural rays, and which showed the importance of the fibrillar structure of the core region. However, while morphing beams inspired from fin rays can duplicate some of their key mechanisms, their structures pale in comparison to the sophisticated morphology of natural rays (figure 1(b)). For example, ray-like synthetic structures typically duplicate the tapered geometry of natural rays [33, 42], but the mechanical properties of the individual hemitrichs and of the core region are uniform along the length of the ray. Natural rays, on the other hand, display gradients of properties in the hemitrich, their cross-section decreasing towards the end of the ray [20, 25, 43]. While there are no direct measurements of gradients in the core region, the density of the collagen fibrils may vary along the length of natural rays, which would also affect morphing and stiffening properties. Gradients of properties and structures are indeed common in natural materials and they have critical implications in terms of functionality and mechanical performance [44–48]. For this study, we hypothesized that gradient in structures and/or properties along the ray contribute to enhancing their morphing and stiffening performance. To explore this hypothesis we designed, fabricated and tested synthetic rays with different combinations of graded properties. We then used the experimental results, in combination with non-linear finite element models, to assess the benefits and limitations of graded properties in ways which are not possible from studying natural fin rays only, and which suggest enhanced designs for fin-inspired morphing structures.

2. Synthetic fin ray design and fabrication

In this study, we designed, fabricated and tested synthetic fin rays with the overall dimensions shown in figure 2. The hemitrichs were fabricated from 0.5 mm thick polymethyl-methacrylate (PMMA, Rowmark, OH, USA) sheets, with a measured flexural modulus $E_\mathrm{h} = 1$ GPa. The individual hemitrichs were laser cut from the sheet using an 80 W CO_2 precision laser cutter (Nova35, Thunder Laser Systems, TX, USA), and dimensions were then verified using an optical microscope (Leica DM2700 M). The dimensions of the uniform hemitrichs were $L = 200$ mm $\times$ $w = 21.5$ mm $\times$ $t_\mathrm{h} = 0.5$ mm. A wider region was added at the base of each hemitrich for clamping to the mechanical testing platform. The core region was designed as an array of rubber ligaments to duplicate the structure of the collagen fibrils in natural fin rays. This structure was laser cut from 1.6 mm thick rubber sheets (RubberCal, CA, USA) with a measured tensile modulus $E_\mathrm{r} = 1.52$ MPa. For this study, we varied the density and arrangement of the ligaments, but their individual cross-section was maintained at 1.6 mm by 1.6 mm for all designs. The two hemitrichs were first manually assembled and glued with cyanoacrylate near their ends to a 5° PMMA wedge, and the core region was then manually glued between the hemitrichs. This provided a robust method to produce synthetic rays with a 5° taper that duplicated the taper of individual natural rays.

The design shown in figure 2 has uniform hemitrichs (the cross-section of the hemitrichs is uniform) and a uniform core (the spacing between the ligaments is uniform), which served as the reference for this study. We then enriched this design with combinations of graded properties in the hemitrichs, and graded properties in the core region as shown in figure 3. To introduce graded properties in the hemitrichs, we tapered their width, using $w = 40$ mm at the base and $w = 3$ mm at the tip of the ray. These dimensions were chosen so that the volume of the individual uniform and tapered hemitrichs were identical (2150 mm^3). The process of tapering the hemitrich from the uniform reference could, therefore, be interpreted as 'moving' material from the end region to the base region, with the total volume kept constant. This 'constant volume' approach was important so we could focus on the effect of gradients. Changing the total volume of the hemitrichs across different designs would bias the comparison because the volume of the individual hemitrichs also affects their stiffness.

The other design enrichment we considered was a non-uniform, graded spacing of the ligaments. The total number of ligaments was maintained at 17 for all designs, but their density (and spacing) was modified by either making them closer near the base of the ray and more spaced near the end (generating a negative gradient of ligament density), or by making them closer near the end of the ray and more spaced near the base (generating a positive gradient of ligament density). Figure 4 shows examples of rays with uniform and graded core regions. These uniform and graded core designs were used in combination with uniform hemitrichs and tapered hemitrichs (figure 3). The numbers of ligaments we considered in the design ranged from 13 to 23 (13, 15, 20 and 23). Designs with less than 13 ligaments were mechanically unstable: under morphing loads or transverse loads, the hemitrichs buckled because of lack of transverse support. On the other hand, designs with more than 23 ligaments resulted in poor morphing, with deformations concentrated near the base of the ray.

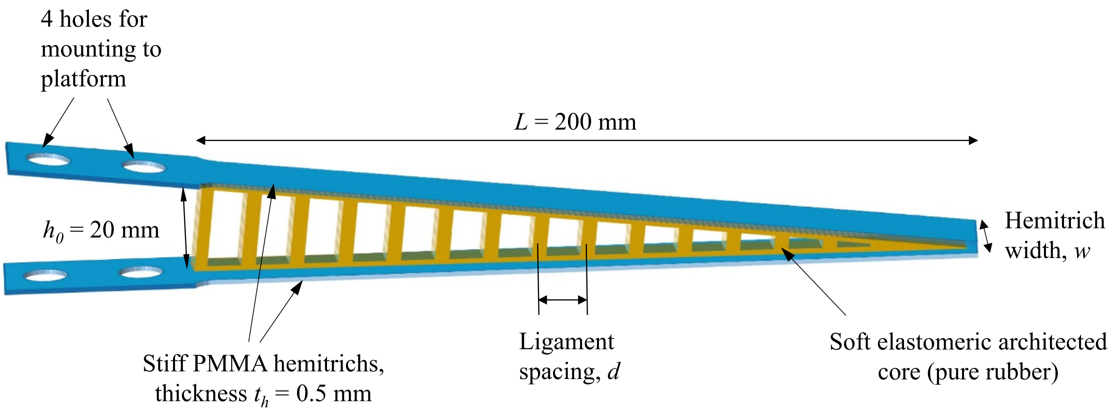

Figure 2. Overall design and dimensions of the synthetic fin rays used in this study.

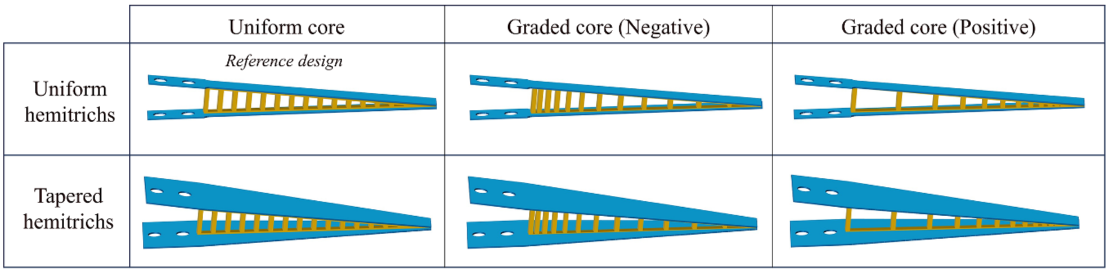

Figure 3. Table showing the six different combinations of ray designs we considered for this study.

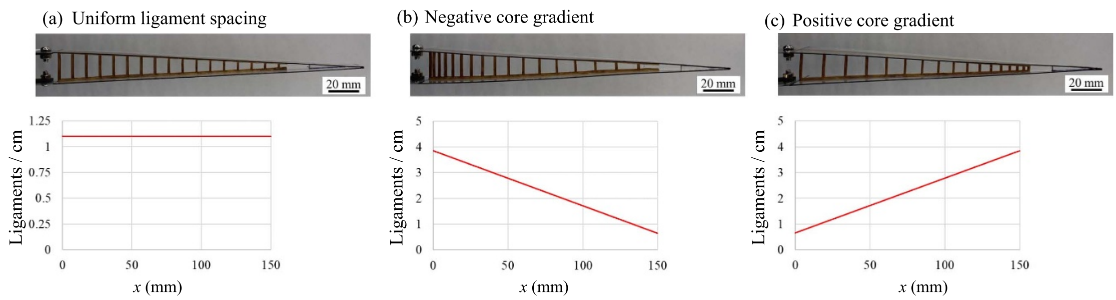

Figure 4. Three different arrangements for the ligaments we considered in this study: (a) uniform ligament spacing; (b) negative core gradient (the density of ligament decreases towards the tip of the ray); (c) positive core gradient (the density of ligament increases towards the tip of the ray). The total number of ligaments (17) is held constant for each of the three designs.

3. Mechanical testing

We measured the stiffness and the morphing performance of the synthetic rays using the instrumented multi-axis micromechanical testing platform shown in figure 5. The displacements were controlled with precision transducers (SOLO Single Axis Manipulator Controller, Sutter Instrument, CA, USA) and the forces were recorded using a load cell (REB7 Subminiature Load Cell, 5 kg capacity, Loadstar Sensors, CA, USA) installed in line with the transducer. To produce consistent and repeatable mechanical responses, rubber must be pre-conditioned with cyclic loading [49] and therefore, once the rays were assembled, they were deformed five times by push-pulls at the base before performing the actual mechanical experiments. We used this setup to perform 'pure morphing' experiments and 'cantilever deflection' experiments described below. Over the course of the experiment, digital images were captured at regular intervals using a DSLR camera (Canon EOS Rebel T6) controlled by a custom MATLAB routine [25, 42, 50]. These images were then post-processed using a custom image analysis MATLAB code to determine the profile ('elastica') of each hemitrich at different stages of loading [25, 42, 50].

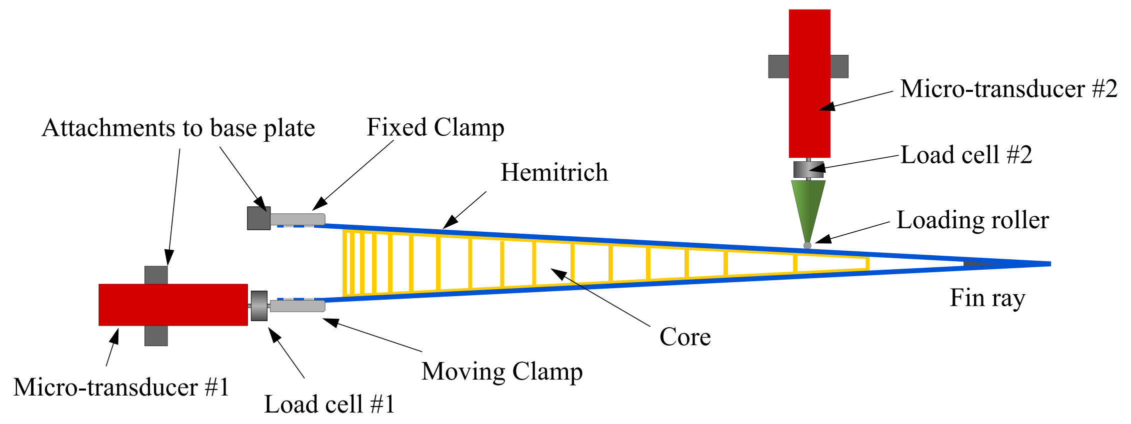

Figure 5. Schematic of the experimental platform used to measure the stiffness and morphing characteristics of the synthetic rays.

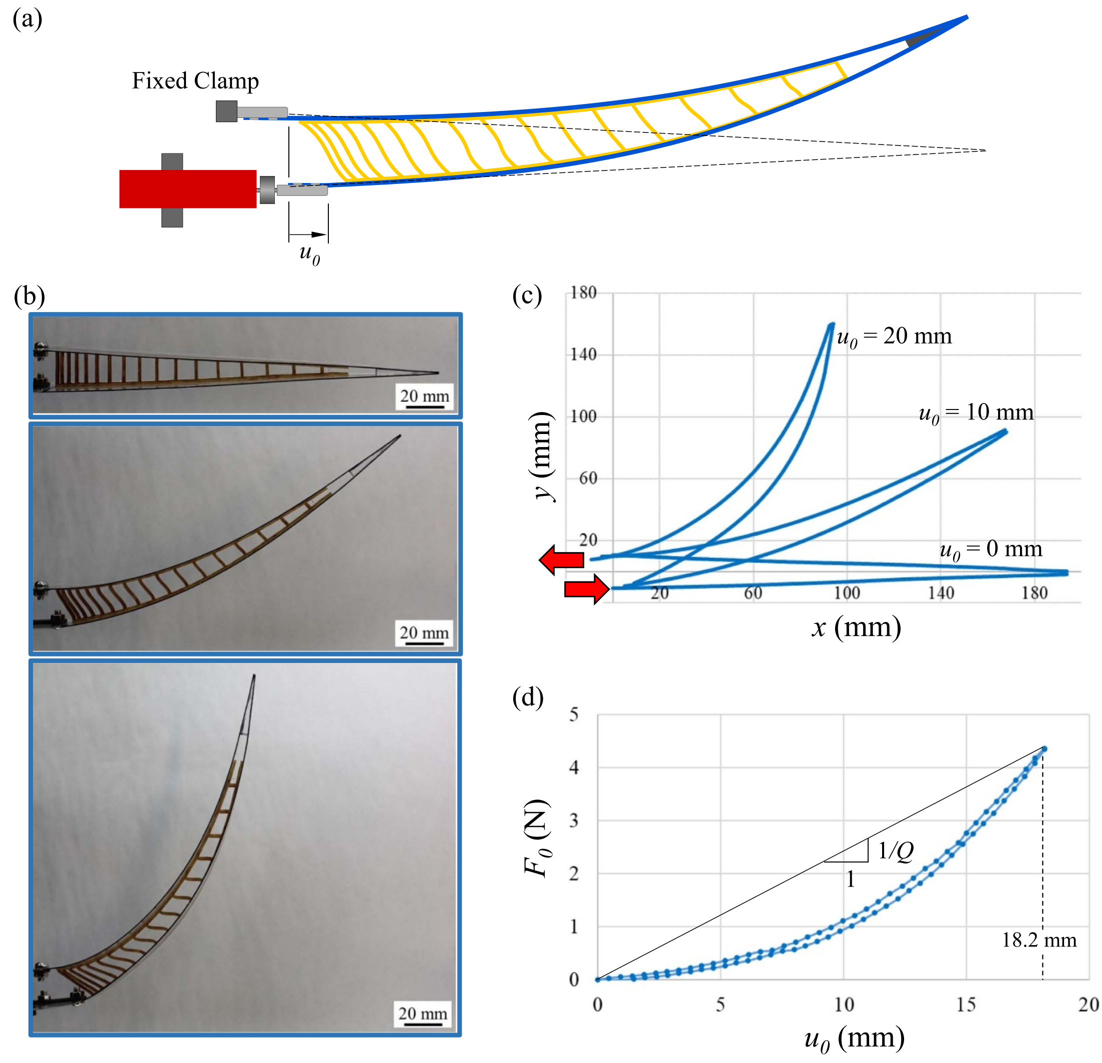

Figure 6. Typical results from morphing experiments: (a) schematic showing pure morphing of a synthetic fin ray; (b) snapshots of morphed rays at three different displacements at the base ($u_0 = 0$ mm, 10 mm and 20 mm); (c) morphed profiles (elastica) at different u_0 values; (d) typical actuation force–displacement (F_0–u_0) curve and the secant slope method used to measure the morphing compliance Q.

3.1. Morphing test

In the 'pure morphing' test, the base of the upper hemitrich was clamped and a push or pull displacement u_0 was imposed on the base of the lower hemitrich while the actuation force F_0 was recorded (figure 6(a)). We used a maximum actuation distance of $u_0 = 20$ mm to ensure that the rays underwent large deformations, while also ensuring that

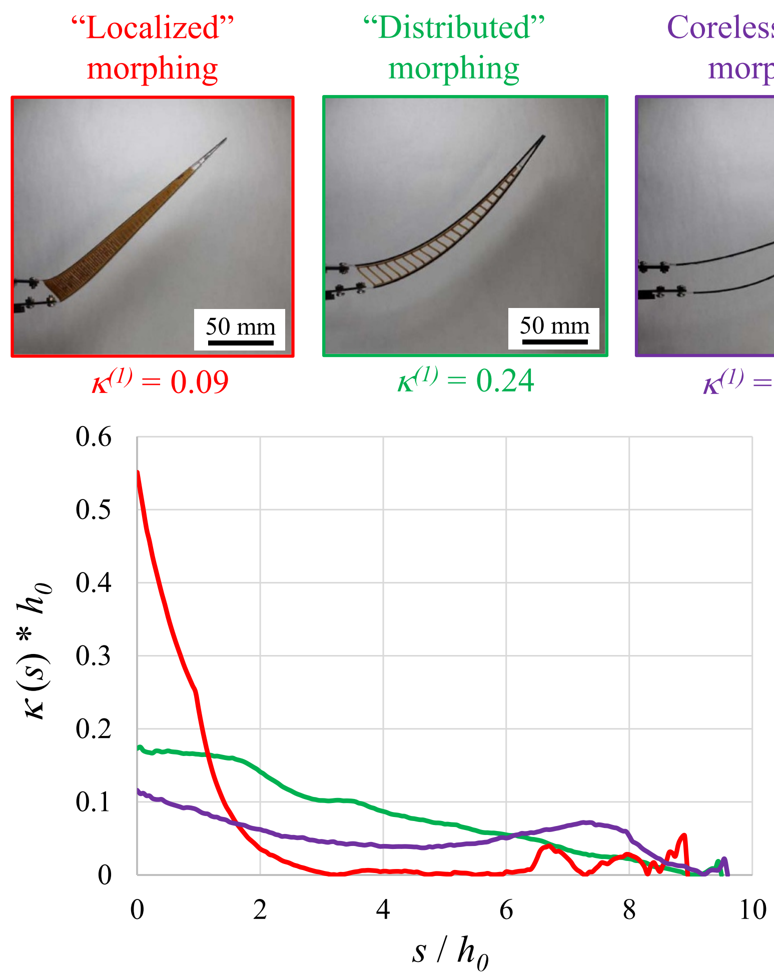

Figure 7. Snapshots of three different ray designs with high density of ligaments leading to 'localized morphing' near the base, optimum core stiffness with about 17 ligaments, and a design with no ligaments that leads to buckling of the lower hemitrichs and poor morphing. The curvature of the ray as function of position along the ray is also shown. This data is then used to compute the first moment of curvature $\kappa^{(1)}$, which we use as a measure of morphing shape.

no failure or damage occurred to the rays during testing. Figure 6(b) shows typical images from this experiment, with the ray gradually morphing to large flexural deformations as u_0 was increased. The exact profile of each hemitrich was computed from image analysis, producing the typical profiles of figure 6(c). A desired morphing behavior is large flexural deformations of the ray propagating over long distances from the base (ideally, morphing occurs over the entire length of the ray). Figure 7 shows how the absence of ligaments in the core leads to buckling and poor morphing. On the other hand, an excessive number of ligaments leads to undesired morphing where the deformations are concentrated near the base. Proper morphing along the entire ray requires a fine balance between the stiffness of the hemitrichs and the stiffness of the core, which we approached for this study by using 17 rubber ligaments. How these ligaments are distributed in the core may also affect the morphed ray, and to capture these more subtle effects, we first measured the local curvature of the ray $\kappa(s)$ at $u_0 = 18.2$ mm, and we then computed the first moment of curvature $\kappa^{(1)}$ [42, 51]:

$$\kappa^{(1)} = \frac{1}{L}\int_0^L s\kappa(s)\,\mathrm{d}s \tag{1}$$

High morphing curvatures far from the base of the ray produce high values of $\kappa^{(1)}$, while the less attractive morphing responses shown in figure 7 lead to low $\kappa^{(1)}$. The $\kappa^{(1)}$ metric provides a robust metric that can be used to measure the overall morphing curvature of each synthetic fin ray [42].

Another important metric for morphing is the actuation force required for morphing. Figure 6(d) shows a typical F_0–u_0 curve. At small actuation displacements, the response is linear with relatively low stiffness, while at larger actuation displacements, stiffening is observed: The rotation and stretching of the ligaments at large deformations increasingly resist shear deformations in the core region. To characterize the force required for morphing based

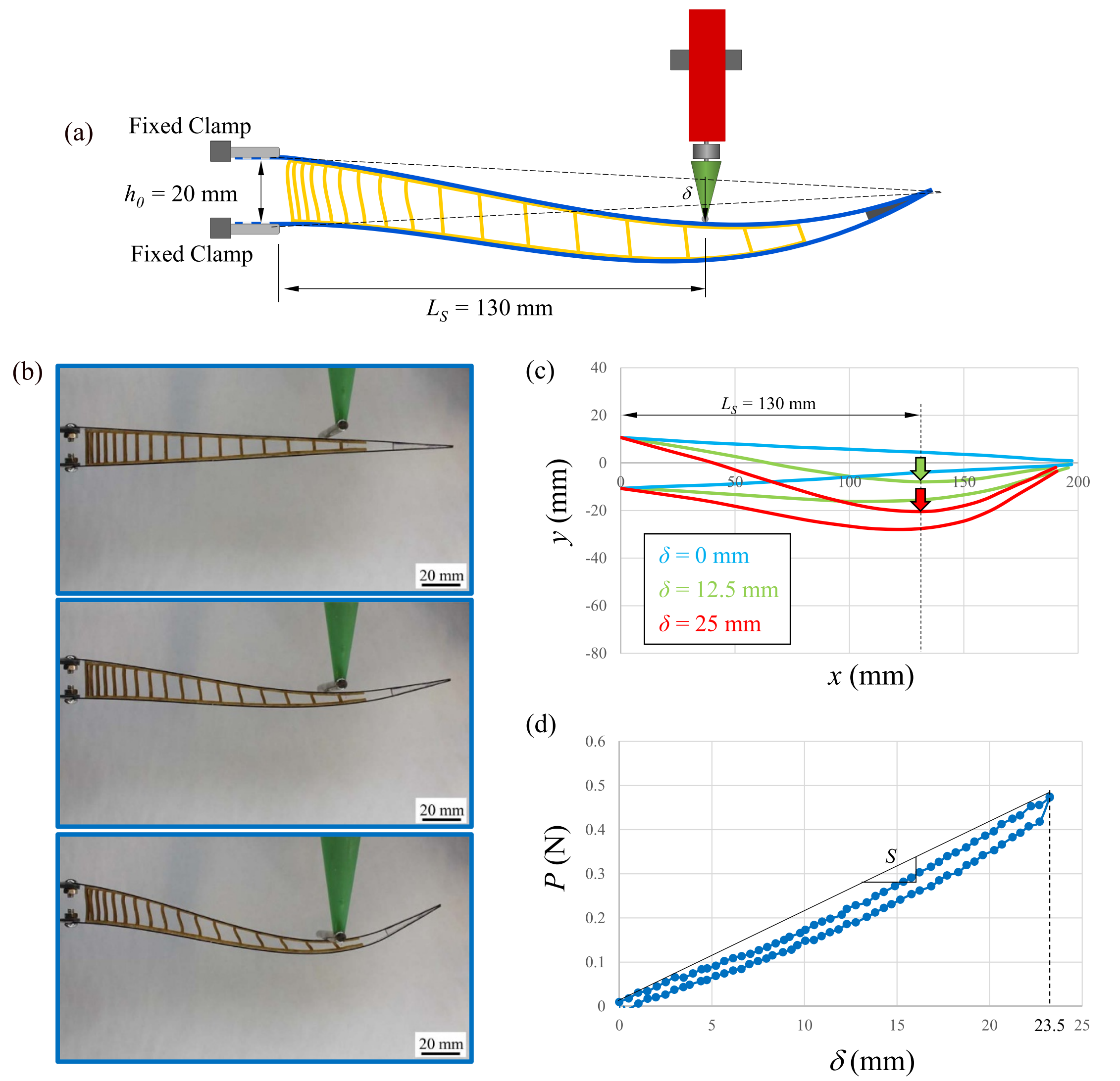

Figure 8. Typical results from flexural experiments: (a) schematic showing the flexural deflection of synthetic fin ray; (b) snapshot of deflected rays; (c) comparison of cantilever elastica at different δ values; (d) typical transverse force–displacement (P–δ) curves and the secant slope method used to measure the flexural stiffness S.

on this nonlinear F_0–u_0 response, we measured the morphing compliance Q for each design based on the slope of the secant line shown in figure 6(d).

3.2. Cantilever deflection

The intent of the 'cantilever deflection' test (figure 8(a)) was to load the ray with a transverse point force applied relatively close to the tip, to duplicate the most traditional and simple way to load a cantilever beam. To this end, the base of each hemitrich was clamped and a controlled transverse deflection δ was imposed at a distance $L_s = 130$ mm from the base, while the corresponding transverse force P was recorded. We used a maximum transverse displacement of $\delta = 25$ mm which ensured that no failure or damage occurred to the rays during testing. Figure 8(b) shows typical snapshots for this experiment. When subjected to a transverse force, the ray responds in a way that is quite different from a regular structural beam. In a regular cantilever beam, the flexural deformation increases near the clamped base because the bending moment is the highest at that point. In contrast, flexural deformations in the ray were concentrated in the region where the transverse force was applied. A major difference between a regular beam and rays is the core region, which in the ray offers little resistance to shear, at least initially. The large shear deformations in the core near the loading nose are visible in figure 8(b), and they result in local flexural deflections. Because of the fused conditions at the end of the ray, the ray bends upwards on the right of the loading nose, so that the very end of the ray appears to deflect very little (this peculiar response is also observed in natural fish fin rays [25]). Figure 8(c) shows the elastica for different levels of deformation, and figure 8(d) shows the force-deflection curve (P–δ curve) for that ray. These curves are typically linear but also show some stiffening at large deformations, which can be explained by the increasing resistance of the core to shearing as the ligaments rotate and stretch

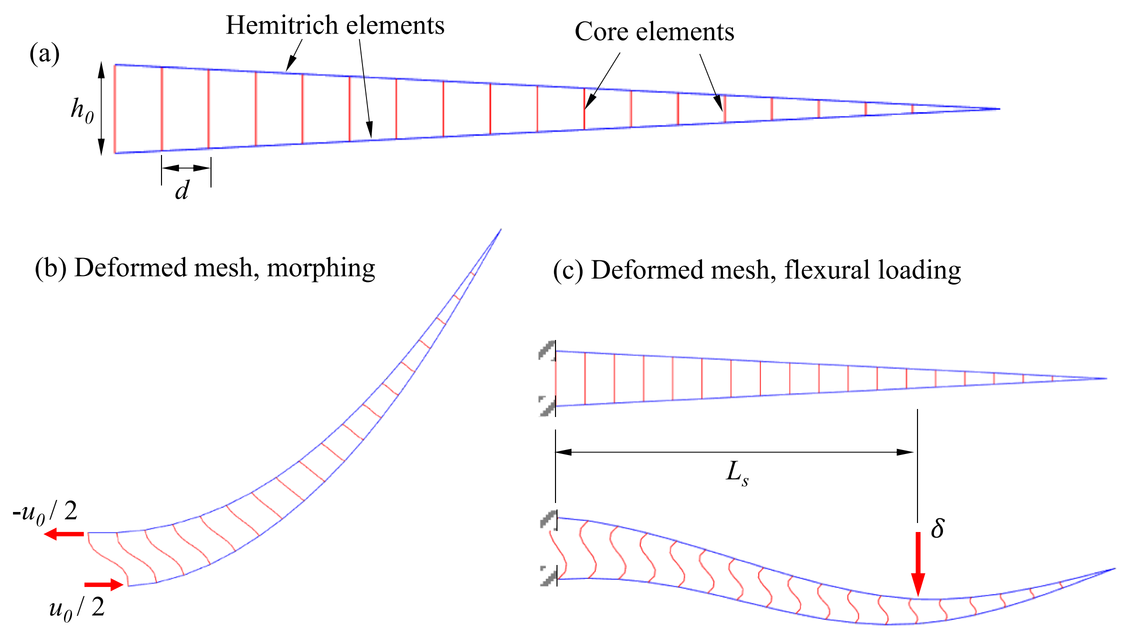

Figure 9. Non-linear finite element model: (a) mesh with nonlinear corotational beam element: stiff blue elements model the hemitrichs, and softer red elements model the ligaments; boundary conditions and typical deformed shapes for (b) morphing and (c) flexural loading.

at large deformations. From the P–δ curve for a given design, we computed a flexural stiffness S, from the slope of the secant modulus shown in figure 8(d).

4. Finite element model

To complement the experimental results and to broaden our understanding of gradients in fish fin rays, we used nonlinear finite element models to capture the mechanics of the rays. The hemitrichs and the ligaments in the core region were modeled with co-rotational beam elements, with elastic properties computed from their cross sections and materials properties (figure 9(a)). The model could either be morphed (figure 9(b)) or deflected by a transverse force (figure 9(c)) to duplicate the experimental setup. More details on the model formulation can be found in [25, 42].

Figure 10 shows typical predictions from the FE model in comparison with the experiments. The model captures the shape of the deformed ray quite accurately, as well as the F_0–u_0 curve, including the nonlinear stiffening effect described above. The model also properly captured the main features of the P–δ flexural curve but slightly underestimated the stiffness, most likely because the boundary conditions in the experiments (mounting at the base, positioning of the loading nose) were not strictly identical to the boundary conditions used in the model. This numerical model is however sufficiently accurate to complement the experiment. In particular, it provides a rapid tool to explore many more designs than in the experiments. For each of these designs, the morphing $\kappa^{(1)}$, the morphing compliance Q and the flexural stiffness S were computed using the same methods as for the experiments.

5. Results

In the experiments, we explored the six different designs shown in figure 3. The experiments were non-destructive, so the same ray could be tested for morphing and cantilever deflection any number of times. To assess the repeatability of the synthetic models and experiment, we fabricated and tested two specimens for each design. Figure 11 shows an overview of the effects of gradients on the three metrics $\kappa^{(1)}$, Q and S as measured experimentally and as predicted by the FE model. In terms of absolute values for these metrics, experiments and FE models are off by up to 20%. However, experiments and FE models are consistent in terms of trends, so the FE models represent a useful tool for the general design of the rays. We first examine the effect of gradients on $\kappa^{(1)}$. Figure 11(a) shows that the ligament gradient density has little effects on $\kappa^{(1)}$, which is consistent with our previous study: as long as the core region is 3–4 orders of magnitude more compliant than the hemitrichs, $\kappa^{(1)}$ is not sensitive to ligament density [42], and this includes the effects of gradient. Tapering the hemitrichs had a much more pronounced effect on $\kappa^{(1)}$, consistently leading to a 40% increase of $\kappa^{(1)}$ compared to rays with uniform hemitrichs. We explain this effect by the lowered flexural stiffness of the hemitrich towards the end of the ray, which promotes flexural deformations away from the base of the rays. We next examine the effect of gradients on the morphing compliance Q

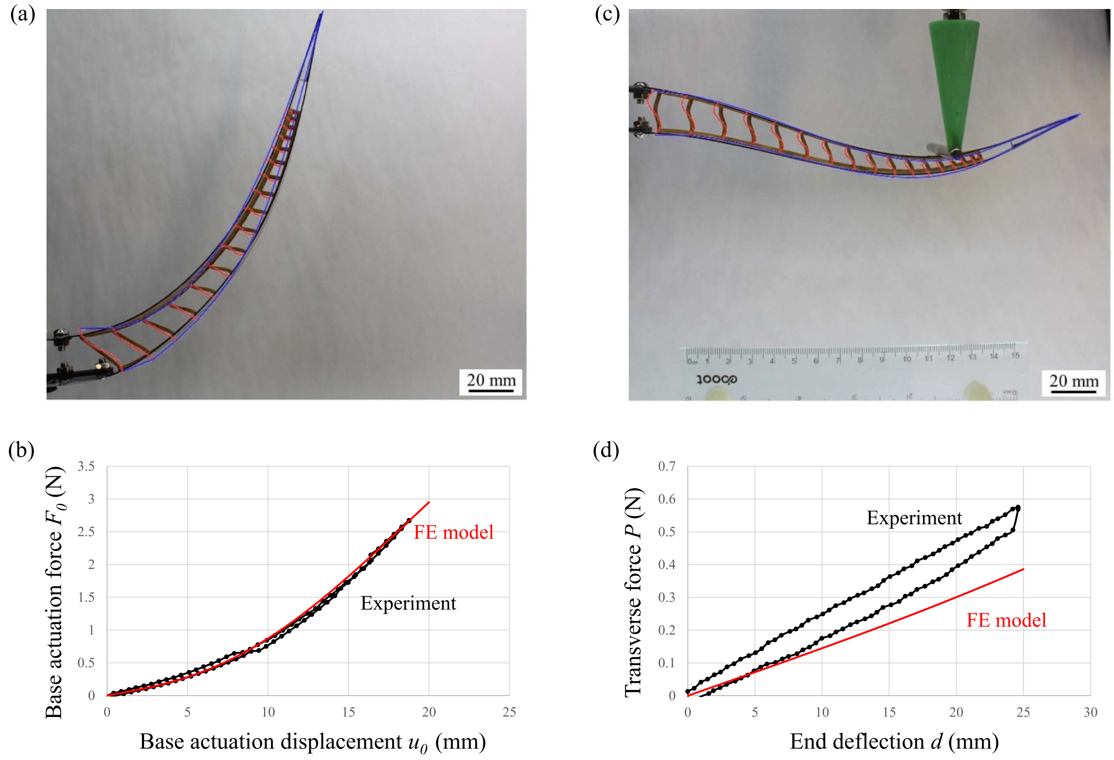

Figure 10. Comparison between experiments and models for a fin ray with tapered hemitrichs and positive core gradient: (a) elastica and (b) F_0–u_0 curves from pure morphing test; (c) elastica and (d) P–δ curves from the flexural test.

(figure 11(b)). Both experiments and models show that Q increases as the ligament gradient density increases from negative to positive values. As the gradient density is increased, the density of ligaments near the base of the ray decreases. Since the base of the ray is the region that experiences the higher shearing from the actuation displacements, lowering the ligament density in this region decreases the actuation force and increases Q. Figure 11(b) also shows that the morphing compliance for rays with tapered hemitrichs is about 20% lower than rays with uniform hemitrichs. Since the large curvatures occur near the base of the ray (figure 6), rays with hemitrichs which are wider at the base require more actuation forces.

Finally, figure 11(c) shows that the flexural stiffness S generally increased as the ligament gradient density is increased. As shown in figure 8, in a typical flexural test, the deformations are concentrated in the region where the transverse load is applied, and stiffening occurs as the ligaments rotate and stretch in that region. Increasing the gradient of ligament density means that more ligaments will be present in this region of high deformation, which in turn leads to increased overall flexural stiffness S. Figure 11(c) shows that rays with tapered hemitrichs have a lower flexural stiffness, which can be explained by the same reason: at the region of high deformations near the application of the point load, the tapered hemitrich is narrower than the uniform hemitrich, which leads to a lower stiffness S overall.

5.1. Design exploration using performance maps

The results presented above show that incorporating gradients in the design of the ray has conflicting effects on $\kappa^{(1)}$, Q and S. This observation is consistent with our previous study, where we used uniform hemitrichs and uniform core regions, but here we focused on varying the density of the ligaments [42]. These previous results showed that increasing the ligament density could decrease $\kappa^{(1)}$, that it consistently increased S but that it also consistently decreased Q. There are, therefore, trade-offs to be made when designing rays with uniform hemitrichs and uniform cores. The question we address here is: can graded properties in the core and/or hemitrichs improve these trade-offs compared to the uniform designs? To answer this question, we explored the design space using finite element models only, because they allow the probing of a very large number of designs. We first set up a reference case where the core and hemitrich regions are uniform, with the overall dimensions of the model shown in figure 2. We varied the ligament density from 0.9 ligaments cm^{-1} to 5.3 ligaments cm^{-1} and for each case we computed $\kappa^{(1)}$, Q and S. We then normalized each of these properties by the property of ray without a core, to obtain the non-dimensional properties $\kappa^{(1)*}$, Q^* and S^*. Figure 12 shows a set of property maps where the axes are S^* and Q^*. Varying the ligament density leads to different combinations of these two properties, which all fall on a single line that clearly shows the trade-off

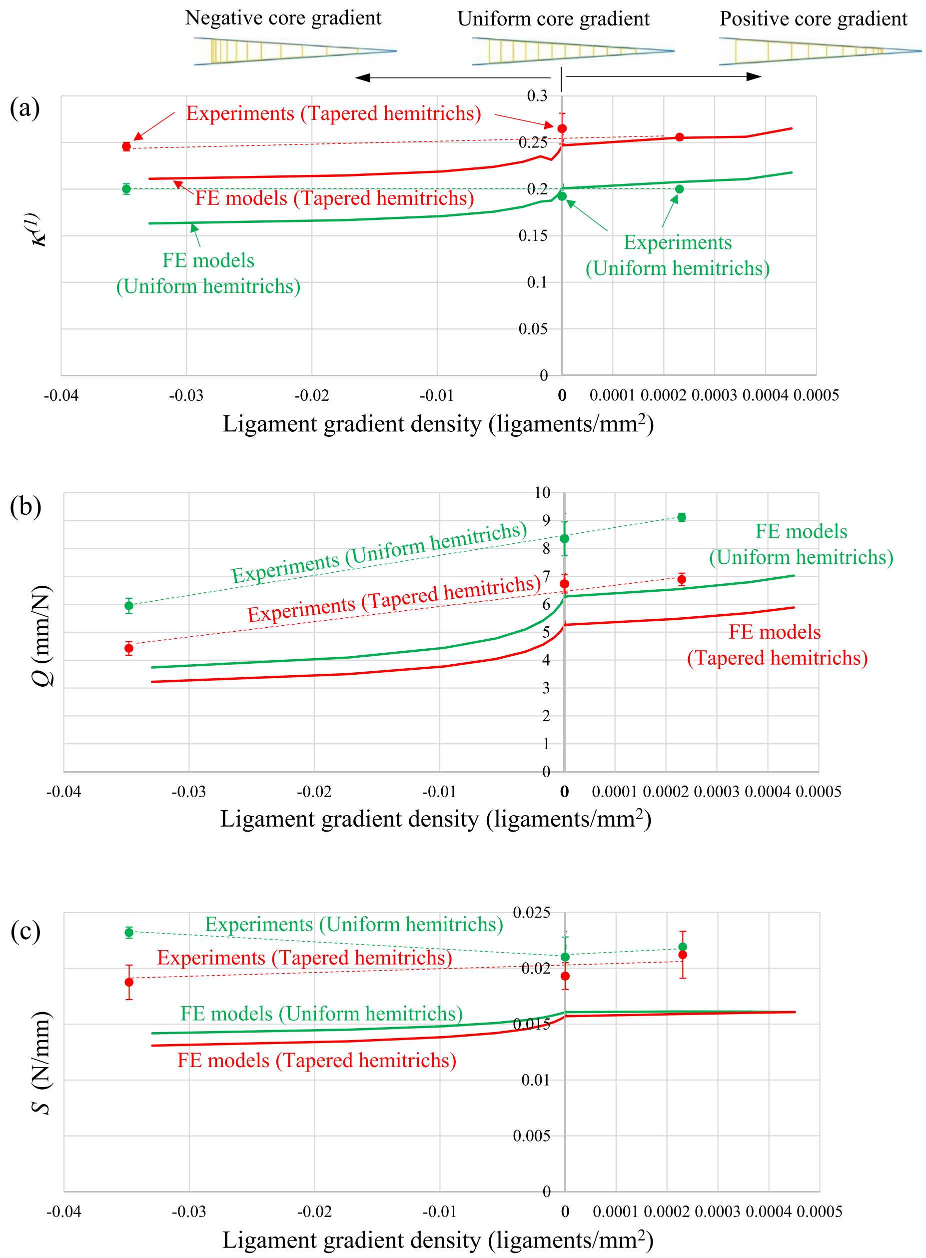

Figure 11. Effect of gradients in the core and hemitrichs on (a) morphing curvature $\kappa^{(1)}$, (b) morphing compliance Q, and (c) structural stiffness S.

between Q^* and S^*. We also show the value of $\kappa^{(1)*}$ as the width of a thin colored region centered on that line.

This reference line for uniform designs confirms that increasing the ligament density decreases $\kappa^{(1)*}$, increases S^* and decreases Q^*. Figure 12(a) also shows the effect of adding a positive or a negative gradient to the spacing of the ligaments (the magnitude of the gradient is the same as figure 4). We first note that the range of properties, particularly stiffness, is different from the uniform case because the gradient creates constraints on the ligament density that can be achieved near the end of the ray (for the positive gradient) or near the base (for the negative gradient). Nevertheless, the map shows that incorporating a positive gradient in the core enables higher combinations of S^* and Q^* compared to the uniform case, and that the range of attainable values for $\kappa^{(1)*}$ is also systematically improved. Incorporating a negative gradient in the core also increases $\kappa^{(1)*}$, but it negatively impacts the possible combinations of S^* and Q^*. Figure 12(b) shows that adding a taper to the hemitrichs decreases the S^* and Q^*, but that it also increases the range of possible $\kappa^{(1)*}$. This decrease can, however, be offset by combining tapered hemitrich gradient with a positive gradient in the core region: figure 12(b) shows that this combination leads to ranges of S^* and Q^* which are slightly lower than the uniform case, but also to significant enhancements for $\kappa^{(1)*}$ with a range of values which is 40%–110% greater than the uniform case.

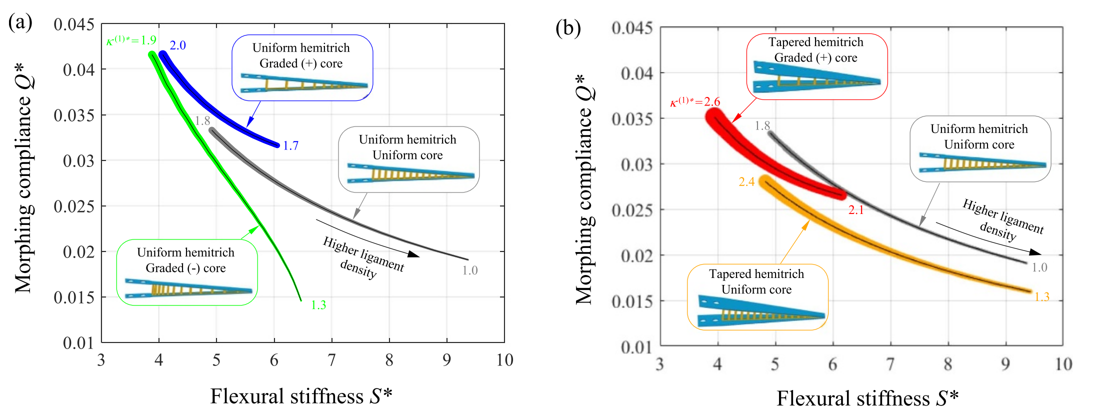

Figure 12. Performance maps obtained from the FE model showing normalized morphing compliance, structural stiffness and morphing curvature: (a) effect of gradient in the core region; (b) effect of gradient in hemitrichs combined with gradients in the core region.

6. Conclusions

The morphing and stiffening performances of natural rays and of bio-inspired synthetic rays are the result of a fine balance between different structural components and properties. Proper morphing can only be achieved within an optimal balance between the flexural stiffness of the hemitrichs and the shear stiffness of the core region. Some of these finer balances can only be assessed by considering regimes of large deformations, for example, the fibrillar structure of the core region is critical to offer the least possible resistance to shearing and morphing at small deformations, while stabilizing the ray and preventing buckling at large deformations. While synthetic morphing only considers uniform compositions and structures for hemitrichs and core regions, natural fish fins (and natural materials in general) display strong gradients which, we hypothesized in this study, could improve morphing and stiffening performance. In this study, we used micromechanical experimental testing and nonlinear FE models to investigate the effects of gradients in the hemitrichs and the core region of the synthetic fin rays. The main conclusions of this study are as follows:

- Increasing the core gradient (the density of ligament is increased towards the tip of the ray) has little effects on $\kappa^{(1)}$. As long as a minimum number of ligaments are present to prevent buckling, an adequate morphing shape is achieved.
- Increasing the core gradient increases the morphing compliance *Q:* positive gradients entail less ligaments near the base of the ray, which makes morphing easier.
- Increasing the core gradient increases the flexural stiffness of the ray *S*: positive gradients entail more ligaments near the end of the ray, which is where most of the deformations occur in the cantilever flexural test (as opposed to traditional cantilever beams where flexural deformations are concentrated near the base of the beam).
- Rays with tapered hemitrichs consistently produce higher $\kappa^{(1)}$. A reduced flexural stiffness in the hemitrichs away from the base promotes flexural deformation from morphing in these areas.
- Rays with tapered hemitrichs lead to lower morphing compliance because wider hemitrichs at the base require more actuation forces, and they also lead to lower stiffness *S* because narrower hemitrichs near the point where the force is applied reduce stiffness in that key area.
- The loss of *Q* and *S* in the rays with tapered hemitrichs can be offset by using graded core regions, which can provide interesting paths to creating rays with high $\kappa^{(1)}$, high *Q* and high *S*.

Natural fish fins suggest new designs for stiff morphing materials that do not require large forces for morphing, yet that can resist deformation or collapse from external loads. In comparison, pneumatic morphing systems that include inflatable fabrics [52] and pneumatic cells [53] require low pressure and forces for morphing, but they suffer from low stiffness. On the other hand, aerospace materials actuated with piezoelectric shear actuators [54] are orders of magnitude stiffer, but they also require high voltages and mechanical forces for morphing. Quantitative comparisons of the stiffness/morphing properties of these systems can be found in [42]. The present study shows that gradients of properties in both the core region and the hemitrichs, therefore, affect the overall morphing and stiffening response of the ray, which demonstrates the importance of this feature for synthetic designs, and which also suggests that gradients have benefits in natural fin rays. Even with these enrichments, the structure of our synthetic rays pale in comparison with natural fin rays (figure 1(b)). Other features that should be explored include segmentations along the hemitrichs, gradients in the length of the segments, tendon effect shown by collagen fibrils at large deformations, non-uniform gradients in the hemitrich/core, or three-dimensional, semi-cylindrical designs for the hemitrichs.

The experimental and modeling methodology presented here can be used to build a comprehensive understanding of the mechanical role of these intricate features. The design guidelines presented here are based on elastic responses which are scale-free, so that the prototypes can be scaled up or down. The relatively simple design and fabrication steps are also amenable to mass production of rays, which can be used in parallel to create morphing structures similar to natural fish fins. Other important properties such as failure by buckling, fracture or fatigue should also be explored to assess the reliability of these structures under extreme, prolonged, and/or cyclic loadings. There are also many possible ways to load the ray mechanically, which depends on the intended function and applications. In this report, we have used a single point force as an 'external load' on the ray, but future experiments could also include multiple point forces, or distributed loads that could duplicate hydrodynamic pressures. Finally, energetic aspects such as the amount of mechanical work needed to achieve specific morphing deformations when the structure is free of external loads or when it is loaded would also possibly reveal new functionalities and design guidelines. The present study nevertheless represents a first step towards design guidelines for more effective stiff morphing materials, with applications in medicine, aerospace, or robotics.

Data availability statement

All data that support the findings of this study are included within the article (and any supplementary files).

Acknowledgments

This research was supported by the College of Engineering and by the Mechanical Engineering department at the University of Colorado Boulder.

ORCID iDs

Saurabh Das https://orcid.org/0009-0009-9553-3259
Francois Barthelat https://orcid.org/0000-0001-8393-3612

References

[1] Ai X, Yue H and Wang W D 2023 Crawling soft robot exploiting wheel-legs and multimodal locomotion for high terrestrial maneuverability *IEEE Trans. Robot.* **39** 1–10
[2] Gopesh T, Wen J H, Santiago-Dieppa D, Yan B, Pannell J S, Khalessi A, Norbash A and Friend J 2021 Soft robotic steerable microcatheter for the endovascular treatment of cerebral disorders *Sci. Robot.* **6** eabf0601
[3] Battaglia M, Sellitto A, Giamundo A, Visone M and Riccio A 2023 Shape memory alloys applied to automotive adaptive aerodynamics *Materials* **16** 4832
[4] Henry A C, Molinari G, Rivas-Padilla J R and Arrieta A F 2019 Smart morphing wing: optimization of distributed piezoelectric actuation *AIAA J.* **57** 2384–93
[5] Mantha S, Pillai S, Khayambashi P, Upadhyay A, Zhang Y, Tao O, Pham H M and Tran S D 2019 Smart hydrogels in tissue engineering and regenerative medicine *Materials* **12** 3323
[6] Koirala S, Prakash S, Karim A and Bhandari B 2023 Shape morphing of foods: mechanism, strategies, and applications *Trends Food Sci. Technol.* **139** 104135
[7] Qiu Y and Park K 2001 Environment-sensitive hydrogels for drug delivery *Adv. Drug. Deliv. Rev.* **53** 321–39
[8] Yao H, Yu M, Fu J, Zhu M, Li Y, Li S, Gan R, Zhou H and Qi S 2023 Shape memory polymers enable versatile magneto-active structure with 4D printability, variable stiffness, shape-morphing and effective grasping *Smart Mater. Struct.* **32** 095005
[9] Zhang Y, Yang J, Liu M and Vella D 2022 Shape-morphing structures based on perforated kirigami *Extreme Mech. Lett.* **56** 101857
[10] Reyssat E and Mahadevan L 2009 Hygromorphs: from pine cones to biomimetic bilayers *J. R. Soc. Interface* **6** 951–7
[11] Castro D and Aharoni H 2023 Shape morphing of planar liquid crystal elastomers *Phys. Rev. Lett.* **130** 178101
[12] Meeussen A S and van Hecke M 2023 Multistable sheets with rewritable patterns for switchable shape-morphing *Nature* **621** 516–20
[13] Li J and Mooney D J 2016 Designing hydrogels for controlled drug delivery *Nat. Rev. Mater.* **1** 1–17
[14] Portela P, Camanho P, Weaver P and Bond I 2008 Analysis of morphing, multi stable structures actuated by piezoelectric patches *Comput. Struct.* **86** 347–56
[15] Reddy J N 1999 On laminated composite plates with integrated sensors and actuators *Eng. Struct.* **21** 568–93
[16] Forterre Y, Skotheim J M, Dumais J and Mahadevan L 2005 How the Venus flytrap snaps *Nature* **433** 421–5
[17] Dakin R, Segre P S, Straw A D and Altshuler D L 2018 Morphology, muscle capacity, skill, and maneuvering ability in hummingbirds *Science* **359** 653–7
[18] Wang W, Lee J-Y, Rodrigue H, Song S-H, Chu W-S and Ahn S-H 2014 Locomotion of inchworm-inspired robot made of smart soft composite (SSC) *Bioinsp. Biomim.* **9** 046006
[19] Fratzl P 2003 Cellulose and collagen: from fibres to tissues *Curr. Opin. Colloid Interface Sci.* **8** 32–39
[20] Alben S, Madden P G and Lauder G V 2007 The mechanics of active fin-shape control in ray-finned fishes *J. R. Soc. Interface* **4** 243–56
[21] Videler J J 1993 *Fish Swimming* (Springer) (https://doi.org/10.1007/978-94-011-1580-3)
[22] Claiborne D H E and B James (eds) 2005 *The Physiology of Fishes* 3rd edn (CRC Press) (https://doi.org/10.1201/9781420058093)
[23] Lauder G V and Madden P G A 2006 Learning from fish: kinematics and experimental hydrodynamics for roboticists *Int. J. Autom. Comput.* **3** 325–35
[24] Lauder G V and Madden P G A 2007 Fish locomotion: kinematics and hydrodynamics of flexible foil-like fins *Exp. Fluids* **43** 641–53
[25] Das S, Hannard F and Barthelat F 2023 Mechanics and properties of fish fin rays in nonlinear regimes of large deformations *Acta Biomater.* **167** 171–81
[26] Hannard F, Mirkhalaf M, Ameri A and Barthelat F 2021 Segmentations in fins enable large morphing amplitudes combined with high flexural stiffness for fish-inspired robotic materials *Sci. Robot.* **6** eabf9710
[27] Wainwright D K and Lauder G V 2020 Tunas as a high-performance fish platform for inspiring the next

generation of autonomous underwater vehicles *Bioinsp. Biomim.* **15** 035007
[28] Triantafyllou M S, Winey N, Trakht Y, Elhassid R and Yoerger D 2020 Biomimetic design of dorsal fins for AUVs to enhance maneuverability *Bioinsp. Biomim.* **15** 035003
[29] Randeni S, Mellin E M, Sacarny M, Cheung S, Benjamin M and Triantafyllou M 2022 Bioinspired morphing fins to provide optimal maneuverability, stability, and response to turbulence in rigid hull AUVs *Bioinsp. Biomim.* **17** 036012
[30] Tangorra J L, Davidson S N, Hunter I W, Madden P G A, Lauder G V, Dong H, Bozkurttas M and Mittal R 2007 The development of a biologically inspired propulsor for unmanned underwater vehicles *IEEE J. Ocean. Eng.* **32** 533–50
[31] Micromachines n.d. A 3D-printed fin ray effect inspired soft robotic gripper with force feedback *Free Full-Text* (available at: www.mdpi.com/2072-666X/12/10/1141) (Accessed 5 November 2023)
[32] Shin J H, Park J G, Kim D I and Yoon H S 2021 A universal soft gripper with the optimized fin ray finger *Int. J. Precis. Eng. Manuf.* **8** 889–99
[33] Crooks W, Vukasin G, O'Sullivan M, Messner W and Rogers C 2016 Fin Ray® effect inspired soft robotic gripper: from the RoboSoft grand challenge toward optimization *Front. Robot.* AI **3** 70
[34] Soft Robotics n.d. Bio-inspired shape-adaptive soft robotic grippers augmented with electroadhesion functionality (available at: www.liebertpub.com/doi/10.1089/soro.2018.0120) (Accessed 5 November 2023)
[35] White C H, Lauder G V and Bart-Smith H 2021 Tunabot Flex: a tuna-inspired robot with body flexibility improves high-performance swimming *Bioinsp. Biomim.* **16** 026019
[36] Curet O M, Patankar N A, Lauder G V and MacIver M A 2011 Mechanical properties of a bio-inspired robotic knifefish with an undulatory propulsor *Bioinsp. Biomim.* **6** 026004
[37] Wolf Z and Lauder G V 2021 A soft robotic model to study the effects of stiffness on fish-like undulatory swimming *Bioinspired Sensing, Actuation, and Control in Underwater Soft Robotic Systems* ed D A Paley and N M Wereley (Springer) pp 153–69
[38] Zhang C W, Zou W, Yu H C, Hao X P, Li G, Li T, Yang W, Wu Z L and Zheng Q 2022 Manta ray inspired soft robot fish with tough hydrogels as structural elements *ACS Appl. Mater. Interfaces* **14** 52430–9
[39] Hou T, Yang X, Su H, Jiang B, Chen L and Wang T 2019 Design and experiments of a squid-like aquatic-aerial vehicle with soft morphing fins and arms *2019 Int. Conf. on Robotics and Automation (ICRA)* pp 4681–7
[40] Chen D, Wu Z, Dong H, Meng Y and Yu J 2023 Platform development and gliding optimization of a robotic flying fish with morphing pectoral fins *Bioinsp. Biomim.* **18** 036010
[41] Li L *et al* 2022 Aerial-aquatic robots capable of crossing the air-water boundary and hitchhiking on surfaces *Sci. Robot.* **7** eabm6695
[42] Das S, Kunjam P, Moling B, Gao T and Barthelat F 2024 Stiff morphing composite beams inspired from fish fins 10.31224/3525
[43] Flammang B E, Alben S, Madden P G A and Lauder G V 2013 Functional morphology of the fin rays of teleost fishes *J. Morphol.* **274** 1044–59
[44] Chen P-Y, Stokes A G and McKittrick J 2009 Comparison of the structure and mechanical properties of bovine femur bone and antler of the North American elk (Cervus elaphus canadensis) *Acta Biomater.* **5** 693–706
[45] Weaver J C *et al* 2010 Analysis of an ultra hard magnetic biomineral in chiton radular teeth *Mater. Today* **13** 42–52
[46] Waite J H, Lichtenegger H C, Stucky G D and Hansma P 2004 Exploring molecular and mechanical gradients in structural bioscaffolds *Biochemistry* **43** 7653–62
[47] Peisker H, Michels J and Gorb S N 2013 Evidence for a material gradient in the adhesive tarsal setae of the ladybird beetle Coccinella septempunctata *Nat. Commun.* **4** 1661
[48] Elbaum R, Zaltzman L, Burgert I and Fratzl P 2007 The role of wheat awns in the seed dispersal unit *Science* **316** 884–6
[49] Tension n.d. Standard test methods for vulcanized rubber and thermoplastic elastomers (available at: www.astm.org/d0412-16r21.html) (Accessed 4 February 2024)
[50] MATLAB 2019 MATLAB version: 9.7 (R2019b) (The MathWorks Inc.)
[51] Yokota K and Barthelat F 2023 Stiff bioinspired architectured beams bend Saint-Venant's principle and generate large shape morphing *Int. J. Solids Struct.* **274** 112270
[52] Gao T, Siéfert E, DeSimone A and Roman B 2020 Shape programming by modulating actuation over hierarchical length scales *Adv. Mater.* **32** 2004515
[53] Gao T, Bico J and Roman B 2023 Pneumatic cells toward absolute Gaussian morphing *Science* **381** 862–7
[54] Baillargeon B P and Vel S S 2005 Active vibration suppression of sandwich beams using piezoelectric shear actuators: experiments and numerical simulations *J. Intell. Mater. Syst. Struct.* **16** 517–30